Mechanics of Materials 140 (2020) 103246

Contents lists available at ScienceDirect

Mechanics of Materials

journal homepage: www.elsevier.com/locate/mechmat

Research paper

Nanoscale mode-III interface crack in a bimaterial with surface elasticity

Ying Yang, Zhen-Liang Hu, Xian-Fang Li*

School of Civil Engineering, Central South University, Changsha 410075, PR China

ARTICLE INFO

Keywords:
Interface crack
Mode-III crack
Surface elasticity
Hypersingular integro-differential equation
Crack-tip field

ABSTRACT

This paper studies a mode-III nanocrack at the interface between two bonded dissimilar materials under anti-plane shear loading. The classical elasticity incorporating surface elasticity is applied to solve a mixed boundary value problem associated with an anti-plane shear interface crack. The influence of surface elasticity on the crack-tip field for a nanoscale mode-III crack is analyzed. By use of the Fourier transform, the problem is reduced to a set of hypersingular integro-differential equations. The displacement and bulk stress jumps are expanded as the Chebyshev orthogonal polynomials and the Galerkin method is used to approximately determine the singular elastic field near the interface crack tips. Consideration of surface elasticity does not cause the disappearance of crack-tip singularity. A usual inverse square-root singularity is derived near the crack tips. The influences of surface elasticity on the stress intensity factor are examined and displayed graphically. The surface residual stress does not alter the stress field for a mode-III interface crack.

1. Introduction

With the fast development of nano/microtechnology in recent years, the mechanical behavior of nanomaterials and nanostructures is particularly significant for a better understanding of small scale structural integrity, reliability, and stability (Del Rio et al., 2015). Due to various causes in fabrication and crystal growth, some defects such as dislocations, grain boundaries, cracks, holes, etc. inevitably appear in materials and structures. These defects often alter the performances of the materials and structures. In particular, experimental evidence shows the size-dependent material properties when the dimension of the structures falls to the nanometer order at least in one direction. A possible explanation of the size-dependence of material properties is attributed to high specific surface area for a nano/micro material or structure. In other words, for nano/micro-scale materials and structures, not only bulk materials but also surface materials affect overall material properties. For macro-materials, the effect of surface phases on the overall properties is so small that it is negligible. For nano-materials, the effect of surface phases cannot be discarded since the contribution becomes relatively large due to high specific surface area for nano/micro materials. Gurtin and Murdoch (1975) and Gurtin et al. (1998) introduced surface/interface elasticity along with surface residual stress to extend the classical theory of elasticity. Based on surface elasticity theory, Ru (2010) put forward a simple geometrical explanation of the surface elasticity and gave several simplified constitutive relations for surface phases. Hu et al. (2014) and Yao and Yun (2012) studied the buckling and vibration of nanowires with the surface effect. Xiao and Li (2018) analyzed the influence of surface elasticity on the flutter and divergence instability of rectangular plates under nonconservative forces. For a circular plate, Yang and Li (2019) addressed the surface effects on bending deflection and natural frequencies for free vibration of a magnetoelectroelastic plate. In addition to surface elasticity and surface residual stress, Zhang et al. (2016) developed an atomistic lattice model to characterize surface relaxation and further applied the nanobeam model to examine the surface effects on the natural frequencies of doubly clamped nanobeams. Using surface elasticity, Dingreville et al. (2005) exploited the surface free energy to describe its effect on the elastic behavior of nano-materials and derived an overall prediction of the material properties of elastic bulk material with nano-sized particles, wires, and films. By means of the complex potential method, Mogilevskaya et al. (2008) studied the interaction of elastic fields of multiple circular nano-inhomogeneities or/and nanopores in a two-dimensional elastic medium. The free transverse vibration of nanobeams with a slanted edge crack was investigated and the influence of the surface phase on the natural frequencies of cracked nanobeams was presented by Hu et al. (2015). Wu (1999) solved the effect of surface stresses on the deformation of an elliptical hole and found the surface stress to change stress intensity factors. Wang et al. (2008) examined the surface effects on the crack-tip stresses for both mode-I and mode-III cracks and found that when the curvature radius of a blunt crack front decreases to nanometers, surface energy strongly affects the stress intensities near the crack tip. For a mode-II

* Corresponding author.
E-mail address: xfli@csu.edu.cn (X.-F. Li).

https://doi.org/10.1016/j.mechmat.2019.103246
Received 19 September 2019; Received in revised form 9 November 2019; Accepted 10 November 2019
Available online 11 November 2019
0167-6636/

nanoscale crack, Fu et al. (2008) analyzed the surface effects on a mode-II crack-tip field. Utilizing the complex potential method, Kim et al. investigated the effects of surface elasticity for a classical mode-III crack embedded in a linearly elastic material or bi-material (Kim et al., 2010; 2011b) and further extended their results to mode-I and mode-II (interface) cracks for plane deformation (Kim et al., 2011c; 2011a). They found that surface elasticity leads to the disappearance of singular stresses near the crack tip. Later, a careful examination of the end-point boundary condition of the crack tips shows a logarithmic singularity of stresses occurring near the crack tips when surface elasticity at the crack faces is considered (Walton, 2012; Kim et al., 2013). Recently, Li applied the singular integral equation method to give the asymptotic stress field and the usual square-root singularity near the mode-III crack tip was revealed (Li, 2019). Nan and Wang (2012) analyzed that the effect of crack face residual stress on the fracture of nanoscale materials. Wang et al. (2013) employed the beam model to address the influence of surface residual tension on stress intensity factors at the crack tips. Wang and Wang (2013) used the double cantilever beam specimens to capture the influence of surface residual stress on the fracture toughness. For a thin plate with a through crack and a rigid inclusion, the influence of surface elasticity on the full stress field in the plate was analyzed and the stress intensity factors are found to depend on the properties of the surface phase (Hu et al., 2018; Hu and Li, 2018). Duan et al. (2009) commented on some progress of the classical theory of elasticity incorporating surface elasticity. On the other hand, the fundamental solution of a concentrated force at the surface of a half-plane or half-space with consideration of surface stresses as well as surface elasticity has been obtained (Wang and Feng, 2007; Gao et al., 2013; 2014), and this solution can be used to treat a class of contact problems related to surface elasticity.

In this paper, we consider an interface crack between two bonded dissimilar elastic media with consideration of surface elasticity and an emphasis is placed on the influence of surface elasticity on the stress singularity and its intensity factors. When antiplane shear loading is applied, we employ the Fourier integral transform to reduce the problem to two coupled hypersingular integro-differential equations. By use of the Chebyshev polynomial expansion method, the resulting equations are converted to a linear system of algebraic equations. By solving the system of finite unknowns, an approximate solution can be obtained. The interface stresses still exhibit a usual square-root singularity near the crack tips. Surface elasticity strongly affects the singularity intensity of stresses. Numerical results illustrate the strong influence of surface material properties on stress intensity factors. Finally, some conclusions are drawn.

2. Statement of the problem

Consider a nanoscale mode-III interface crack, as shown in Fig. 1. It is assumed that the upper and the lower half-spaces are respectively occupied by two bonded dissimilar homogeneous isotropic materials with a through crack of length $2a$ lying on the interface. For convenience, a Cartesian coordinate system is chosen, and the interface crack is located at $|x| < a, y = 0$ on the x-axis. Apart from the crack segment, two media are perfectly bonded with each other over $|x| \geq a$. In the present study, remote longitudinal shear or antiplane shear loading is exerted at infinity. Since a nanoscale crack is focused, the impact of surface elasticity on the crack faces should be taken into consideration, and this is fundamentally different from the classical case. That is, for linear bulk materials, the bulk stress-strain relations are governed by

$$\sigma_{ij} = \lambda\varepsilon_{ll}\delta_{ij} + 2\mu\varepsilon_{ij}, \tag{1}$$

where λ and μ are the Lamé constants, σ_{ij} Cauchy stress tensor, and ε_{ij} the strain tensor. For linear surface materials, the surface stress-strain relations read (Gurtin and Murdoch, 1975; Murdoch, 1976)

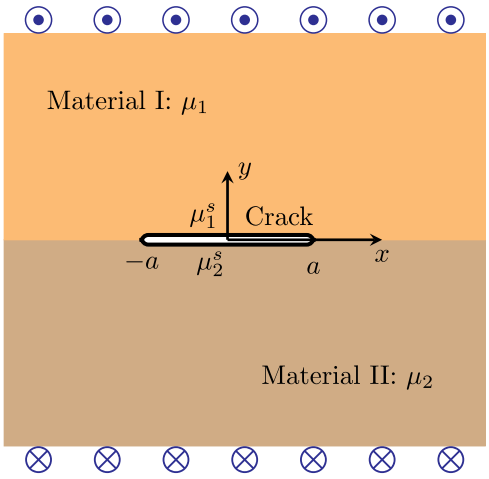

Fig. 1. Schematic of a mode-III interface crack between two dissimilar materials with surface elasticity.

$$\sigma^s_{\alpha\beta} = \sigma_0\delta_{\alpha\beta} + (\lambda^s + \sigma_0)\varepsilon^s_{\gamma\gamma}\delta_{\alpha\beta} + 2(\mu^s - \sigma_0)\varepsilon^s_{\alpha\beta} + \sigma_0 u^s_{\beta,\alpha}, \tag{2}$$

$$\sigma^s_{\alpha 3} = \sigma_0 u^s_{3,\alpha}, \tag{3}$$

where λ^s and μ^s are the surface Lamé constants that are independent of the surface residual stress σ_0, $\sigma^s_{\alpha\beta}$ the Piola-Kirchhoff surface stress tensor, $\varepsilon^s_{\alpha\beta}$ the surface strain tensor, u_i (u^s_α) bulk (surface) elastic displacement vector. In the above, δ_{ij} or $\delta_{\alpha\beta}$ is the Kronecker delta, Latin subscripts i, j, l take values from 1 to 3, and Greek subscripts α, β, γ range from 1 to 2, a comma in the subscript denotes differentiation with respect to the spatial variable following the comma, and the Einstein convention of summation over repeated lower-case indices has been used. A quantity with the superscript s implies the one on the surface phase. In the following analysis, since the surface of zero thickness is bonded to the bulk phase without any slipping and debonding, it is appropriate to assume that at a local position, the surface elastic displacements are identical to the bulk elastic displacements, i.e. $u_\alpha(\mathbf{x}) = u^s_\alpha(\mathbf{x})$ for $x \in S$, S being the surface. Besides, the bulk stresses are related to the surface stresses, and they satisfy the following equilibrium equation (Chen et al., 2006)

$$[[\sigma_{ij}n_i]] + \sigma^s_{\alpha j,\alpha} = 0, \tag{4}$$

where $[[*]] = (*)^+ - (*)^-$ stands for the jump of a quantity across the surface.

For a nanoscale mode-III interface crack through the medium along the z-axis, it is sufficient to limit our attention to an arbitrary plane, the oxy-plane, say. So there is only a unique out-of-plane displacement component, denoted as w, which only depends on spatial variables x and y. In view of (1), antiplane stresses in the bulk phase read

$$\sigma^{(j)}_{xz} = \mu_j w^{(j)}_{,x} \quad \sigma^{(j)}_{yz} = \mu_j w^{(j)}_{,y} \tag{5}$$

where a quantity with the superscript (j) corresponds to the one in the upper ($j = 1$) and lower ($j = 2$) half-planes, μ_1, μ_2 denote the shear moduli of the upper and lower half-planes, respectively. Inserting the constitutive relationships (5) to the equilibrium equation

$$\sigma^{(j)}_{xz,x} + \sigma^{(j)}_{yz,y} = 0 \tag{6}$$

yields the well-known governing equation

$$\nabla^2 w^{(j)} = 0 \tag{7}$$

with ∇^2 is the two-dimensional Laplacian operator.

For a mode-III interface crack lying along the x-axis, the subscripts on the crack faces should take 1 and 3, then from (4) the bulk stresses and the surface stresses at the crack faces meet the following equation

$$\sigma^s_{xz,x} + \sigma^s_{zz,z} + [[\sigma_{yz}]] = 0, \tag{8}$$

where [[*]] specifies the jump across the surface. By virtue of (2), we further rewrite Eq. (8) as

$$\sigma_{yz}^{(1)}(x, 0^+) = q(x) - \mu_1^s w_{,xx}^{(1)}(x, 0^+), \quad |x| < a \tag{9}$$

at the crack upper face and

$$\sigma_{yz}^{(2)}(x, 0^-) = q(x) + \mu_2^s w_{,xx}^{(2)}(x, 0^-), \quad |x| < a \tag{10}$$

at the crack lower face, where μ_j^s is the surface shear modulus of the crack upper and lower faces ($j = 1, 2$), and $\sigma_0^{(j)}$ is the surface residual stresses of the crack upper and lower faces ($j = 1, 2$), $q(x)$ represents the negative of applied antiplane shear loading at the crack faces. For instance, the loading $q(x)$ takes $-\tau^\infty$ for the case of $\sigma_{yz} = \tau^\infty$ at infinity, so the crack faces remain traction-free after superposing the disturbed elastic field induced by the crack to a uniform field in the whole elastic plane without crack. In principle, the disturbed crack-tip field induced by the crack is of particular interest in the study of fracture mechanics, so in the following analysis, we solely analyze the singular elastic field induced by the interface crack with the surface effects. From the above, only the surface shear modulus or surface elasticity affects the crack-tip field and the surface residual stress σ_0 does not bring any variation of the crack-tip field.

3. Derivation of the hypersingular integro-differential equations

Here the Fourier transform technique is applied to convert the associated boundary value problem under scrutiny to a set of hypersingular integro-differential equations. To achieve this, besides the above-stated boundary conditions (9) and (10), the continuity conditions on the interface of two bonded dissimilar materials

$$w^{(1)}(x, 0) = w^{(2)}(x, 0), \quad \sigma_{yz}^{(1)}(x, 0) = \sigma_{yz}^{(2)}(x, 0), \quad |x| > a, \tag{11}$$

are also required.

With the aid of the Fourier transform, we find that appropriate out-of-plane displacements take the following form

$$w^{(1)}(x, y) = \frac{1}{\sqrt{2\pi}} \int_{-\infty}^{\infty} A_1(\xi) e^{-|\xi|y + i\xi x} d\xi, \quad y \geq 0 \tag{12}$$

and

$$w^{(2)}(x, y) = \frac{1}{\sqrt{2\pi}} \int_{-\infty}^{\infty} A_2(\xi) e^{|\xi|y + i\xi x} d\xi, \quad y \leq 0 \tag{13}$$

where $i = \sqrt{-1}$, $A_j(\xi)(j = 1, 2)$ are unknown functions in ξ to be determined from the boundary conditions. With these expressions for the out-of-plane displacements, using (5) we give the expressions for the bulk stresses at the crack plane below

$$\sigma_{yz}^{(1)}(x, y) = -\frac{\mu_1}{\sqrt{2\pi}} \int_{-\infty}^{\infty} |\xi| A_1(\xi) e^{-|\xi|y + i\xi x} d\xi, \tag{14}$$

$$\sigma_{yz}^{(2)}(x, y) = \frac{\mu_2}{\sqrt{2\pi}} \int_{-\infty}^{\infty} |\xi| A_2(\xi) e^{|\xi|y + i\xi x} d\xi. \tag{15}$$

To solve the problem easily, we introduce two new auxiliary functions $g(x)$ and $h(x)$ such that

$$2g(x) = w^{(1)}(x, 0) - w^{(2)}(x, 0), \quad 2h(x) = \sigma_{yz}^{(1)}(x, 0) - \sigma_{yz}^{(2)}(x, 0), \tag{16}$$

where $2g(x)$ corresponds to the displacement jump across the crack faces, while $2h(x)$ corresponds to the bulk Cauchy stress jump across the crack faces in the bulk material. Because of consideration of surface stresses, bulk stresses are no longer continuous across the crack faces, which may be seen from (9) and (10). Nonetheless, if the surface phase is neglected, there is no stress jump across the crack faces and continuous bulk stresses are anticipated. It is worth noting that at the crack-free part of the interface, the elastic displacement and bulk stresses are both continuous. That is to say

$$g(x) = 0, \quad h(x) = 0, \quad |x| \geq a. \tag{17}$$

Making use of the continuity conditions (11) or (17) one gets

$$\frac{1}{\sqrt{2\pi}} \int_{-\infty}^{\infty} [A_1(\xi) - A_2(\xi)] e^{i\xi x} d\xi = \begin{cases} 0, & |x| > a \\ 2g(x), & |x| < a \end{cases} \tag{18}$$

$$\frac{1}{\sqrt{2\pi}} \int_{-\infty}^{\infty} [\mu_1 A_1(\xi) + \mu_2 A_2(\xi)] |\xi| e^{i\xi x} d\xi = \begin{cases} 0, & |x| > a \\ -2h(x), & |x| < a. \end{cases} \tag{19}$$

Recalling the identity

$$\int_{-\infty}^{\infty} e^{-ix\xi} dx = 2\pi\delta(\xi) \tag{20}$$

where $\delta(\xi)$ is the Dirac delta function, we perform the Fourier transform to both sides of Eq. (18) and obtain

$$A_1(\xi) - A_2(\xi) = \sqrt{\frac{2}{\pi}} \int_{-a}^{a} g(s) e^{-i\xi s} ds. \tag{21}$$

Similarly, from Eq. (19) we have

$$\mu_1 A_1(\xi) + \mu_2 A_2(\xi) = -\sqrt{\frac{2}{\pi}} \frac{1}{|\xi|} \int_{-a}^{a} h(s) e^{-i\xi s} ds. \tag{22}$$

Solving (21) and (22) we can express A_1 and A_2 in terms of the introduced functions $g(x)$ and $h(x)$

$$A_1(\xi) = \frac{1}{\mu_1 + \mu_2} \sqrt{\frac{2}{\pi}} \left[\mu_2 \int_{-a}^{a} g(s) e^{-i\xi s} ds - \frac{1}{|\xi|} \int_{-a}^{a} h(s) e^{-i\xi s} ds \right], \tag{23}$$

$$A_2(\xi) = -\frac{1}{\mu_1 + \mu_2} \sqrt{\frac{2}{\pi}} \left[\mu_1 \int_{-a}^{a} g(s) e^{-i\xi s} ds + \frac{1}{|\xi|} \int_{-a}^{a} h(s) e^{-i\xi s} ds \right]. \tag{24}$$

In order to determine A_1 and A_2, we need to apply the boundary conditions (9) and (10). To this end, it is convenient to express $\sigma_{yz}^{(j)}(x, y)$, $w_{,xx}^{(j)}$ in terms of $g(x)$ and $h(x)$. We substitute (23) into (14), after some manipulations, to get

$$\begin{aligned} \sigma_{yz}^{(1)}(x, y) &= -\frac{\mu_1}{\pi(\mu_1 + \mu_2)} \left[i\mu_2 \int_{-a}^{a} g(s) ds \frac{d}{ds} \int_{-\infty}^{\infty} \frac{|\xi|}{\xi} e^{-|\xi|y + i\xi(x-s)} d\xi - \right. \\ &\quad \left. \int_{-a}^{a} h(s) ds \int_{-\infty}^{\infty} e^{-|\xi|y + i\xi(x-s)} d\xi \right] \\ &= -\frac{2\mu_1}{\pi(\mu_1 + \mu_2)} \left[\mu_2 \int_{-a}^{a} g(s) \frac{d}{ds} \left[\frac{s - x}{(s - x)^2 + y^2} \right] ds - \right. \\ &\quad \left. \int_{-a}^{a} \frac{y h(s)}{(s - x)^2 + y^2} ds \right] \end{aligned} \tag{25}$$

where we have used the following well-known integrals

$$\int_0^{\infty} \exp(-\xi|y|) \sin(\xi x) d\xi = \frac{x}{x^2 + y^2}, \tag{26}$$

$$\int_0^{\infty} \exp(-\xi|y|) \cos(\xi x) d\xi = \frac{|y|}{x^2 + y^2}. \tag{27}$$

If introducing a complex variable $z = x + iy$, which does not bring any confusion with the subscript z, we can express (25) in terms of the complex variable z. Accordingly, one has

$$\begin{aligned} \sigma_{yz}^{(1)}(x, y) &= \frac{\mu_1 \mu_2}{\pi(\mu_1 + \mu_2)} \int_{-a}^{a} \left[\frac{g(s)}{(s - z)^2} + \frac{g(s)}{(s - \bar{z})^2} \right] ds \\ &\quad - \frac{i\mu_1}{\pi(\mu_1 + \mu_2)} \int_{-a}^{a} \left[\frac{h(s)}{s - z} - \frac{h(s)}{s - \bar{z}} \right] ds \end{aligned} \tag{28}$$

for $y \geq 0$, i.e. $\mathrm{Im}(z) \geq 0$, where $\bar{z}$ denotes the conjugate of the complex variable z.

In a similar manner, the bulk stresses in the lower half-plane can also be derived, e.g.

$$\sigma_{yz}^{(2)}(x,y)=\frac{\mu_1\mu_2}{\pi(\mu_1+\mu_2)}\int_{-a}^{a}\left[\frac{g(s)}{(s-z)^2}+\frac{g(s)}{(s-\bar{z})^2}\right]ds - \frac{i\mu_2}{\pi(\mu_1+\mu_2)}\int_{-a}^{a}\left[\frac{h(s)}{s-z}-\frac{h(s)}{s-\bar{z}}\right]ds \tag{29}$$

for $y\le 0$, i.e. $\mathrm{Im}(z)\le 0$.

Taking into account

$$\lim_{\epsilon\to 0^+}\frac{1}{x\pm i\epsilon}=\frac{1}{x}\mp i\pi\delta(x) \tag{30}$$

we let $z\to x$, i.e. $y\to 0^{\pm}$, in Eqs. (28)and (29) and find that the interface stress $\sigma_{yz}^{(j)}(x,0)$ become

$$\sigma_{yz}^{(1)}(x,0^+)=\frac{2\mu_1\mu_2}{\pi(\mu_1+\mu_2)}\int_{-a}^{a}\frac{g(s)}{(s-x)^2}ds+\frac{2\mu_1}{\mu_1+\mu_2}h(x), \tag{31}$$

$$\sigma_{yz}^{(2)}(x,0^-)=\frac{2\mu_1\mu_2}{\pi(\mu_1+\mu_2)}\int_{-a}^{a}\frac{g(s)}{(s-x)^2}ds-\frac{2\mu_2}{\mu_1+\mu_2}h(x). \tag{32}$$

On the other hand, using the result (20) and (26), from (12) we get

$$w_{,xx}^{(1)}(x,0^+)=\frac{2\mu_2}{\mu_1+\mu_2}g''(x)-\frac{2}{\pi(\mu_1+\mu_2)}\int_{-a}^{a}\frac{h(s)}{(s-x)^2}ds, \tag{33}$$

where a prime denotes differentiation with respect to x. An analogous treatment to $w_{,xx}^{(2)}(x,0)$ allows us to arrive at

$$w_{,xx}^{(2)}(x,0^-)=-\frac{2\mu_1}{\mu_1+\mu_2}g''(x)-\frac{2}{\pi(\mu_1+\mu_2)}\int_{-a}^{a}\frac{h(s)}{(s-x)^2}ds. \tag{34}$$

Substituting (31)-(34) into the boundary conditions (9) and (10) leads to

$$\frac{\mu_2}{\pi}\int_{-a}^{a}\frac{g(s)}{(s-x)^2}ds+h(x)+\frac{\mu_1^s}{\mu_1}\left[\mu_2 g''(x)-\frac{1}{\pi}\int_{-a}^{a}\frac{h(s)}{(s-x)^2}ds\right]=\frac{1}{2}\left(1+\frac{\mu_2}{\mu_1}\right)q(x),\quad |x|<a, \tag{35}$$

$$\frac{\mu_1}{\pi}\int_{-a}^{a}\frac{g(s)}{(s-x)^2}ds-h(x)+\frac{\mu_2^s}{\mu_2}\left[\mu_1 g''(x)+\frac{1}{\pi}\int_{-a}^{a}\frac{h(s)}{(s-x)^2}ds\right]=\frac{1}{2}\left(1+\frac{\mu_1}{\mu_2}\right)q(x),\quad |x|<a. \tag{36}$$

Due to the hypersingular nature of the kernel $1/(s-x)^2$ in (35) and (36), the coupled Eqs. (35) and (36) form a set of hypersingular integro-differential equations. Here hypersingular integral is understood in the sense of Hadamard finite-part integral (Kaya and Erdogan, 1987). The hypersingular integral equation method has been widely used to tackle crack problems in a 2D plane (Chan et al., 2003; Li et al., 2013). For certain special cases, the well-known singular integral equations can be recovered. For example, if neglecting surface elasticity, implying $\mu_j^s=0$, from (35) and (36) one has

$$h(x)+\frac{\mu_2}{\pi}\int_{-a}^{a}\frac{g(s)}{(s-x)^2}ds=\frac{1}{2}\left(1+\frac{\mu_2}{\mu_1}\right)q(x),\quad |x|<a, \tag{37}$$

$$-h(x)+\frac{\mu_1}{\pi}\int_{-a}^{a}\frac{g(s)}{(s-x)^2}ds=\frac{1}{2}\left(1+\frac{\mu_1}{\mu_2}\right)q(x),\quad |x|<a. \tag{38}$$

After multiplying (37) by μ_1 and multiplying (38) by μ_2, we subtract (37) from (38) and arrive at $h(x)=0$, which implies $\sigma_{yz}^{(1)}(x,0)=\sigma_{yz}^{(2)}(x,0)$ at the interface, as expected. Each of (37) and (38) with $h(x)=0$ reduces to the hypersingular integral equation for a mode-III interface crack of a bi-material derived by Kaya and Erdogan (1987).

For another special case, if two dissimilar elastic media are identical, we have $\mu_1^s=\mu_2^s$, $\sigma_0^{(1)}=\sigma_0^{(2)}$, $\mu_1=\mu_2$, Eqs. (35) and (36) simplify to

$$h(x)-\frac{\mu^s}{\pi\mu}\int_{-a}^{a}\frac{h(s)}{(s-x)^2}ds=0 \tag{39}$$

$$\mu^s g''(x)+\frac{\mu}{\pi}\int_{-a}^{a}\frac{g(s)}{(s-x)^2}ds=q(x). \tag{40}$$

Obviously, Eq. (40) retrieves the one for a nanoscale mode-III crack embedded in an elastic medium (Li, 2019). For Eq. (39), it is easily found that it has only a trivial solution (Hori and Nemat-Nasser, 1990; Martin, 1992).

Alternatively, since $g(\pm a)=0$ and $h(\pm a)=0$ imply the single value conditions of the out-of-plane displacement and bulk stresses at the crack tips, after integration by parts for hypersingular terms, we also rewrite Eqs. (35) and (36) as a set of singular integro-differential equations

$$\frac{1}{\pi}\int_{-a}^{a}\frac{g'(s)}{s-x}ds+\frac{\mu_1^s}{\mu_1}g''(x)+\frac{1}{\mu_2}\left[h(x)-\frac{\mu_1^s}{\mu_1}\frac{1}{\pi}\int_{-a}^{a}\frac{h'(s)}{s-x}ds\right]=\frac{1}{2}\left(\frac{1}{\mu_1}+\frac{1}{\mu_2}\right)q(x), \tag{41}$$

$$\frac{1}{\pi}\int_{-a}^{a}\frac{g'(s)}{s-x}ds+\frac{\mu_2^s}{\mu_2}g''(x)-\frac{1}{\mu_1}\left[h(x)-\frac{\mu_2^s}{\mu_2}\frac{1}{\pi}\int_{-a}^{a}\frac{h'(s)}{s-x}ds\right]=\frac{1}{2}\left(\frac{1}{\mu_1}+\frac{1}{\mu_2}\right)q(x), \tag{42}$$

where $|x|<a$. In the following, we will solve the hypersingular integro-differential Eqs. (35) and (36).

4. Solution to the integro-differential equations

In this section, we turn our attention to seeking suitable solutions of the resulting hypersingular integro-differential equations. For convenience of analysis, we introduce the following dimensionless quantities

$$\bar{h}(\bar{x})=h(x),\quad \bar{g}(\bar{x})=\frac{g(x)}{a},\quad \zeta(\bar{x})=\frac{q(x)}{\tau_0}, \tag{43}$$

$$\bar{x}=\frac{x}{a},\quad \bar{s}=\frac{s}{a},\quad \beta_j=\frac{\mu_j^s}{a\mu_j}, \tag{44}$$

where τ_0 is the stress reference value.

Since $\bar{g}(\bar{x})$ and $\bar{h}(\bar{x})$ stand for the dimensionless out-of-plane displacement jump and bulk stress jumps across the crack faces, it is easy to find that both of them have the constraint conditions (17), i.e.

$$\bar{g}(\pm 1)=0,\quad \bar{h}(\pm 1)=0. \tag{45}$$

In order to solve the above-resulting hypersingular integro-differential Eqs. (35) and (36), according to the above-introduced dimensionless quantities, it is convenient to rewrite them as a normalized form

$$\beta_1\bar{g}''(\bar{x})+\frac{1}{\pi}\int_{-1}^{1}\frac{\bar{g}(\bar{s})}{(\bar{s}-\bar{x})^2}d\bar{s}+\frac{1}{\mu_2}\left[\bar{h}(\bar{x})-\frac{\beta_1}{\pi}\int_{-1}^{1}\frac{\bar{h}(\bar{s})}{(\bar{s}-\bar{x})^2}d\bar{s}\right]=\frac{1}{2}\left(\frac{1}{\mu_1}+\frac{1}{\mu_2}\right)\tau_0\zeta(\bar{x}), \tag{46}$$

$$\beta_2\bar{g}''(\bar{x})+\frac{1}{\pi}\int_{-1}^{1}\frac{\bar{g}(\bar{s})}{(\bar{s}-\bar{x})^2}d\bar{s}-\frac{1}{\mu_1}\left[\bar{h}(\bar{x})-\frac{\beta_2}{\pi}\int_{-1}^{1}\frac{\bar{h}(\bar{s})}{(\bar{s}-\bar{x})^2}d\bar{s}\right]=\frac{1}{2}\left(\frac{1}{\mu_1}+\frac{1}{\mu_2}\right)\tau_0\zeta(\bar{x}), \tag{47}$$

where $|\bar{x}|<1$.

As pointed out in Li (2019), it seems unlikely to obtain an exact solution to hypersingular integro-differential Eqs. (46) and (47), even for the exact singularity near the crack tips. In the following, using the

Galerkin method, we appeal to the Chebyshev polynomials to approximate the desired solution. First, we rewrite (46) and (47) in the following form

$$\frac{1}{\pi}\int_{-1}^{1}\frac{\bar{g}(\bar{s})}{\bar{s}-\bar{x}}d\bar{s}+\frac{\mu_1\beta_2+\mu_2\beta_1}{\mu_1+\mu_2}\bar{g}'(\bar{x}) + \frac{\beta_2-\beta_1}{\pi(\mu_1+\mu_2)}\int_{-1}^{1}\frac{\bar{h}(\bar{s})}{\bar{s}-\bar{x}}d\bar{s}=\frac{1}{2}\tau_0\left(\frac{1}{\mu_1}+\frac{1}{\mu_2}\right)\zeta^*(\bar{x}), \tag{48}$$

$$\frac{\mu_1\beta_2+\mu_2\beta_1}{\mu_1+\mu_2}\bar{h}(\bar{x})-\frac{\beta_1\beta_2}{\pi}\int_{-1}^{1}\frac{\bar{h}(\bar{s})}{(\bar{s}-\bar{x})^2}d\bar{s} + \frac{\beta_2-\beta_1}{\pi(\mu_1^{-1}+\mu_2^{-1})}\int_{-1}^{1}\frac{\bar{g}(\bar{s})}{(\bar{s}-\bar{x})^2}d\bar{s}=\frac{1}{2}(\beta_2-\beta_1)\tau_0\zeta(\bar{x}), \tag{49}$$

where $|\bar{x}|<1$. The corresponding details are given in Appendix A.

Furthermore, since the solution $\bar{g}(\bar{x})$ and $\bar{h}(\bar{x})$ have asymptotic behavior like $\sqrt{1-\bar{x}^2}$ as $\bar{x}$ is close to 1 (see Appendix B), a suitable solution to Eqs. (48) and (49) can be expanded as Chebyshev polynomials of the second kind:

$$\bar{g}_N(\bar{x})=\frac{1}{2}\tau_0\left(\frac{1}{\mu_1}+\frac{1}{\mu_2}\right)\sqrt{1-\bar{x}^2}\sum_{n=0}^{N}b_nU_n(\bar{x}), \tag{50}$$

$$\bar{h}_N(\bar{x})=\frac{1}{2}\tau_0\sqrt{1-\bar{x}^2}\sum_{n=0}^{N}c_nU_n(\bar{x}), \tag{51}$$

where b_n and c_n are constants to be determined through appropriate conditions, N is a positive integer, which is chosen so large that $\bar{g}_N(\bar{x})$ and $\bar{h}_N(\bar{x})$ converge to the desired true solution, $T_n(\bar{x})$ and $U_n(\bar{x})$ are respectively Chebyshev polynomials of the first kind and the second kind, defined by

$$T_n(\bar{x})=\cos[n\cos^{-1}(\bar{x})],\quad n=0,1,2,\ldots \tag{52}$$

$$U_n(\bar{x})=\frac{\sin[(n+1)\cos^{-1}(\bar{x})]}{\sin[\cos^{-1}(\bar{x})]},\quad n=0,1,2,\ldots \tag{53}$$

Recalling some closed-form integral and derivative formulas, we obtain the following linear algebraic equations for the unknown constants b_n and c_n ($n=0,1,\ldots,N$) (the detailed procedure is given in Appendix C).

$$\sum_{n=0}^{N}\left[\frac{\mu_1\beta_2+\mu_2\beta_1}{\mu_1+\mu_2}\frac{(n+1)\pi}{2}\delta_{mn}+a_{mn}^{+}\right]b_n + \frac{\mu_1\mu_2(\beta_2-\beta_1)}{(\mu_1+\mu_2)^2}\sum_{n=0}^{N}a_{mn}^{+}c_n=-f_{1m} \tag{54}$$

$$-\sum_{n=0}^{N}\frac{(n+1)\pi}{2}(\beta_2-\beta_1)\delta_{mn}b_n + \sum_{n=0}^{N}\left[\frac{\mu_1\beta_2+\mu_2\beta_1}{\mu_1+\mu_2}a_{mn}^{-}+\frac{(n+1)\pi}{2}\beta_1\beta_2\delta_{mn}\right]c_n=(\beta_2-\beta_1)f_{2m} \tag{55}$$

where $m=0,1,\ldots N$, δ_{mn} denotes the Kronecker symbol, and

$$a_{mn}^{\pm}=\frac{1+(-1)^{m-n}}{2}\left[\frac{1}{1-(m-n)^2}\pm\frac{1}{1-(m+n+2)^2}\right], \tag{56}$$

$$f_{1m}=\int_{-1}^{1}\zeta^*(\bar{x})T_{m+1}(\bar{x})d\bar{x},\quad \zeta^*(\bar{x})=\int_{0}^{\bar{x}}\zeta(\bar{s})d\bar{s}, \tag{57}$$

$$f_{2m}=\int_{-1}^{1}\zeta(\bar{x})U_m(\bar{x})\sqrt{1-\bar{x}^2}d\bar{x}. \tag{58}$$

Therefore, Eqs. (54) and (55) form a linear system of $2(N+1)$ algebraic equations with $2(N+1)$ unknowns. It is straightforward to solve the above system through a standard method, and the desired solution can be then determined. Once the coefficients b_n and c_n are determined, the entire stress field in the upper and lower half-plane can be obtained by inserting (50) and (51) into (28) and (29), respectively. For example, with the help of the following integral results

$$\frac{1}{\pi}\int_{-1}^{1}\frac{\sqrt{1-t^2}U_n(t)}{t-\zeta}dt=-(\zeta-\sqrt{\zeta^2-1})^{n+1}, \tag{59}$$

$$\frac{1}{\pi}\int_{-1}^{1}\frac{\sqrt{1-t^2}U_n(t)}{(t-\zeta)^2}dt=\frac{(n+1)(\zeta-\sqrt{\zeta^2-1})^{n+1}}{\sqrt{\zeta^2-1}}, \tag{60}$$

where $\zeta\notin(-1,1)$ is a complex variable, and $\sqrt{\zeta^2-1}$ is understood as a branch of taking real as ζ is real and larger than unity, we have the stress $\sigma_{yz}(x,y)$ in the upper and lower half-planes

$$\sigma_{yz}^{(j)}(x,y)=\frac{\tau_0}{2}\sum_{n=0}^{N}\frac{(n+1)b_n}{a^n}\left[\frac{(z-\sqrt{z^2-a^2})^{n+1}}{\sqrt{z^2-a^2}}+\frac{(\bar{z}-\sqrt{\bar{z}^2-a^2})^{n+1}}{\sqrt{\bar{z}^2-a^2}}\right] + \frac{\tau_0}{2}\frac{i\mu_j}{\mu_1+\mu_2}\sum_{n=0}^{N}\frac{c_n}{a^{n+1}}[(z-\sqrt{z^2-a^2})^{n+1}-(\bar{z}-\sqrt{\bar{z}^2-a^2})^{n+1}]. \tag{61}$$

In particular, of much interest is the stress field at the interface. To get the interface stress, by setting $z=x$ ($x\notin[-a,a]$), one acquires the interface stress at the crack-free part, e.g.

$$\sigma_{yz}^{(1)}(x,0)=\sigma_{yz}^{(2)}(x,0) =\tau_0\sum_{n=0}^{N}(n+1)b_n\left[\frac{x}{a}-\sqrt{\left(\frac{x}{a}\right)^2-1}\right]^{n+1}\left[\sqrt{\left(\frac{x}{a}\right)^2-1}\right]^{-1},\quad x>a. \tag{62}$$

For $x<-a$, the symmetry allows one to immediately determine the bulk stress $\sigma_{yz}^{(1)}(x,0)$. It is obvious from the above result that bulk stress still exhibits an inverse square-root singularity. In addition, due to the influence of the surface stress, in view of (28), (29), and (30), if using

$$\frac{1}{\pi}\int_{-1}^{1}\frac{U_n(\bar{s})\sqrt{1-\bar{s}^2}}{(\bar{s}-\bar{x})^2}d\bar{s}=-(n+1)U_n(\bar{x}),\quad |\bar{x}|<1, \tag{63}$$

one obtains the stresses at the crack faces

$$\sigma_{yz}^{(1)}(\bar{x},0)=-\tau_0\sum_{n=0}^{N}\left[(n+1)b_n-\frac{\mu_1\sqrt{1-\bar{x}^2}}{\mu_1+\mu_2}c_n\right]U_n(\bar{x}),\quad |\bar{x}|<1, \tag{64}$$

$$\sigma_{yz}^{(2)}(\bar{x},0)=-\tau_0\sum_{n=0}^{N}\left[(n+1)b_n+\frac{\mu_2\sqrt{1-\bar{x}^2}}{\mu_1+\mu_2}c_n\right]U_n(\bar{x}),\quad |\bar{x}|<1, \tag{65}$$

and they are indeed not equal.

From the above analytic expression for the interface stresses at $y=0$, we easily determine stress intensity factor K_{III} at the crack tip $x=\pm a$, defined by

$$K_{III}^{\pm}=\lim_{|x|\to a^+}\sqrt{2\pi|x\mp a|}\,\sigma_{yz}^{(1)}(x,0). \tag{66}$$

Upon the substitution of (62) into (66), one gets

$$K_{III}^{+}=\tau_0\sqrt{\pi a}\sum_{n=0}^{N}(n+1)b_n,\quad K_{III}^{-}=\tau_0\sqrt{\pi a}\sum_{n=0}^{N}(n+1)(-1)^nb_n. \tag{67}$$

Note that since the unknown constants b_n and c_n depend on the parameters β_n, as seen from Eqs. (54) and (55), the stress intensity factors are affected by both bulk and surface shear moduli, but independent of surface residual tension. It is interesting to note that Kim et al. (2011b) applied different assumptions to solve a similar problem based on the complex variable method and found the nonsingular stresses near the crack tips.

Table 1
The normalized stress intensity factor $K_{III}/\tau_0\sqrt{\pi a}$.

β	N = 80	N = 100	N = 200
10^{-8}	0.999916	0.999869	0.999485
10^{-6}	0.991669	0.987129	0.951178
10^{-4}	0.562309	0.462943	0.221235
10^{-3}	0.168227	0.132117	0.0639105
10^{-2}	0.0492867	0.039375	0.0196685
10^{-1}	0.0143603	0.0115109	0.00577972

5. Numerical results and discussion

This section is devoted to the examination of the influence of surface elasticity on stress intensity factor and stress distribution through numerical examples. To carry out our calculations, the material properties of the surface phase must be provided. According to the estimate of Sharma and Ganti (2004), the surface parameters can be approximately predicted by the following transformation: $\mu^s = \mu t$, t being the thickness of about 1∼2 lattice spacing and chosen as 5 Å in the present paper, and the upper half-plane is occupied by Ag with bulk shear modulus $\mu_1 = 23.6$ GPa and the lower half-plane by Pt with shear modulus $\mu_2 = 59.7$ GPa (Shenoy, 2005).

The following numerical results are only presented for uniform remote loading, i.e. $q(x) = -\tau_0$. First, to confirm the convergence of our method, let us consider a special case of two bonded materials reducing to identical material. In this case, we have $\mu_1 = \mu_2$, $\beta_1 = \beta_2$. Using (55), one gets $c_n = 0$ and from (54) one acquires

$$\sum_{n=0}^{N}\left[\frac{(2n+1)\pi}{2}\beta\delta_{mn} + a_{mn}^{+}\right]b_n = \frac{2}{3-4m(1+m)}, \quad m = 0, 1, \ldots N. \tag{68}$$

It is clear that the coefficients b_n are dependent on the parameter β alone. By solving the above linear equations, the b_n's are determined and the stress intensity factors are given by (67). Table 1gives the numerical results of the normalized stress intensity factor $K_{III}/\tau_0\sqrt{\pi a}$ for different values of N and β. Since (50) and (51) are expanded as an orthogonal polynomial with weight, the first N-term coefficients b_n and c_n are unchanged when the term number N is raised. The obtained results are in agreement with those given by Li (2019). From Table 1, one finds that for $\beta = 10^{-8}$, meaning that surface effect is nearly negligible, the normalized stress intensity factors are equal to unity. It means when the crack length arrives at a macro scale such as cm or larger, the value of β is close to 10^{-8} and the classical stress intensity factor is recovered. Moreover, for such β values, the convergence of the numerical results is very rapid. However, with the crack length decreasing, or β rising, we find that the surface effect is enhanced, and there is obvious declination in the normalized stress intensity factors. Moreover, the convergence rate becomes quite slow for larger values of β. For example, if $\beta = 0.1$, $K_{III}/\tau_0\sqrt{\pi a} = 0.0115109$ if taking $N = 100$ and 0.00577972 if taking $N = 200$. In fact, the exact value should be zero since it only exhibits a logarithmic singularity, not the inverse square-root singularity (Walton, 2012; Kim et al., 2013).

In the following numerical results, we give the normalized stress intensity factor $K_{III}^{\pm}/\tau_0\sqrt{\pi a}$ for various values of the upper and lower surface parameters β_1 and β_2 with Ag occupying the upper half-plane and Pt occupying the lower half-plane, respectively. For two bonded dissimilar materials, the normalized stress intensity factors drop with the increase of β_1, as viewed in Table 2. This conclusion is similar to that for an identical material with a nano crack. Also, the numerical results converge well for small values such as $\beta_1 = 10^{-8}$ while the convergence rate becomes quite slow with the increase of β_1. In the following calculation, $N = 200$ is chosen unless otherwise stated.

After the coefficients b_n and c_n are determined by solving the resulting algebraic equations, the out-of-plane displacement jump $\bar{g}(\bar{x})$ and bulk stress jump $\bar{h}(\bar{x})$ across the crack faces can be calculated through the expansion (50) and (51), and the corresponding profiles at the crack-face with $\beta_2 = 3\beta_1$ are plotted in Fig. 2. From Fig. 2, one finds that the introduction of the surface effect significantly changes the behavior of the out-of-plane displacement jumps at the crack tips. However, if β_1 is less than 10^{-3}, the surface properties have little influence on the crack-face displacement jump. The influence progressively becomes more sensitive when β_1 is greater than 10^{-3}.

For an interfacially cracked bimaterial subjected to tensile loading, the crack-tip field exhibits oscillatory behavior in the context of linear elastic fracture mechanics (England, 1965), and oscillatory singularity does not take place when subjected to compression-shear loading (Li et al., 2015b; 2015a). For mode-III interface cracks, the stresses are always continuous across the crack-free interface and show a square-root singularity near the crack tips. Although a square-root singularity remains, the bulk stresses are no longer continuous across the crack faces. Fig. 3 clearly demonstrates the stress jump across the crack faces. Moreover, the jump magnitude at the crack faces is related to the position.

Figs. 4 –7 show the variation of the upper and lower bulk stresses $\sigma_{yz}^{(1)}(x, 0)/\tau_0$, $\sigma_{yz}^{(2)}(x, 0)/\tau_0$ as a function of x for $\beta_2 = 3\beta_1$. From Fig. 4, it is seen that the bulk stresses nearly take different constants at the upper and lower crack faces for a bimaterial with $\beta_1 = 10^{-4}$. However, with β_1 rising, the surface effect alters the distribution of the bulk stresses on the crack faces. For example, for $\beta_1 = 10^{-2}$, 10^{-1}, it is seen from Figs. 6 and 7 that the bulk stresses on the upper and lower crack faces are not constant, but vary. At the crack-free part, the bulk stress exhibits an inverse square-root singularity and the crack-tip stress becomes sufficiently large, as shown in Figs. 4–7. Due to two bonded dissimilar materials, it is anticipated that the anti-plane shear bulk stress components are not symmetric on the upper and lower crack faces, but equal on the crack-free interface thanks to the continuity of stress.

As mentioned before, the stresses near the crack tips and stress intensity factors are always size-dependent. Therefore, to reflect the influence of the crack length on the stress intensity factors, in what follows we plot the variation of the stress intensity factors against the crack half-length a in Fig. 8. For comparison, we also calculate the corresponding results when two dissimilar materials reduce to an identical material, and the evaluated results are represented by the dashed lines in Fig. 8(a,b). From Fig. 8a, for a cracked bimaterial with

Table 2
The normalized stress intensity factor $K_{III}^{\pm}/\tau_0\sqrt{\pi a}$ with $\beta_2/\beta_1 = 3$.

β_1	N = 80	N = 100	N = 200	N = 300	N = 400	N = 500
10^{-8}	0.999868	0.999795	0.999192	0.998192	0.996800	0.995018
10^{-6}	0.987007	0.980021	0.926652	0.852469	0.770377	0.689550
10^{-4}	0.483869	0.393025	0.186331	0.119540	0.0879992	0.0696899
10^{-3}	0.141324	0.111268	0.0541122	0.0358423	0.0268168	0.0214290
10^{-2}	0.0410039	0.0327784	0.0163896	0.0109326	0.00820284	0.00656419
10^{-1}	0.0111371	0.00892800	0.00448343	0.00299353	0.00224690	0.00179837

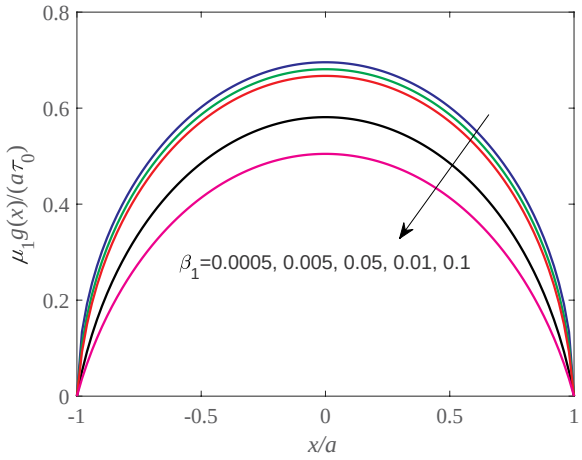

Fig. 2. Profile of the out-of-plane displacement jump parameter $\bar{g}(\bar{x})/\tau_0$ across the crack face of a bimaterial with $\beta_2 = 3\beta_1$.

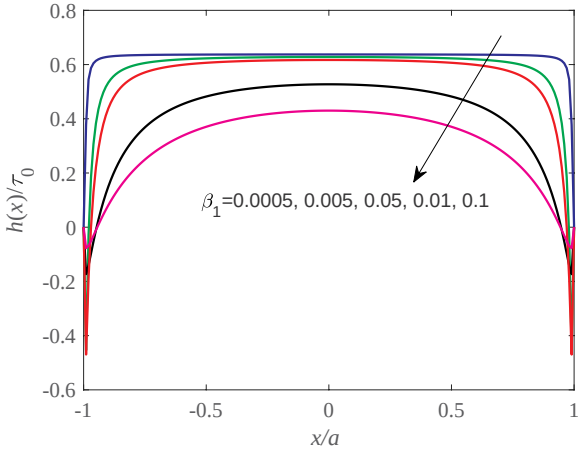

Fig. 3. Profile of the out-of-plane stress jump parameter $\bar{h}(\bar{x})/\tau_0$ across the crack face of a bimaterial with $\beta_2 = 3\beta_1$.

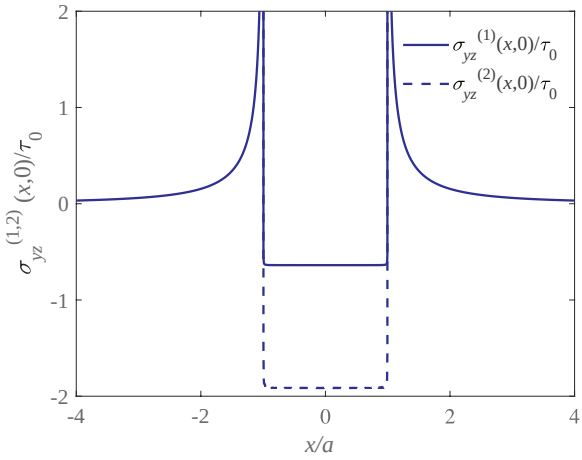

Fig. 4. Variation of the bulk stresses at the crack line as a function of x for a bimaterial with $\beta_2 = 3\beta_1$ and $\beta_1 = 10^{-4}$.

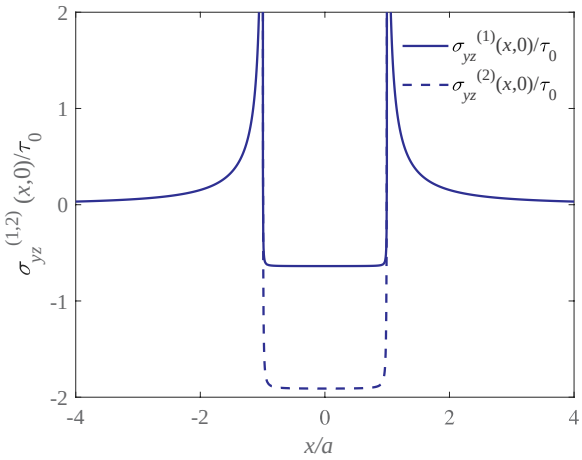

Fig. 5. Variation of the bulk stresses at the crack line as a function of x for a bimaterial with $\beta_2 = 3\beta_1$ and $\beta_1 = 10^{-3}$.

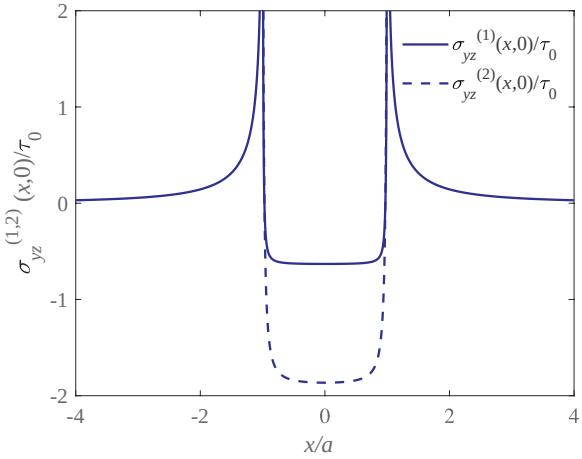

Fig. 6. Variation of the bulk stresses at the crack line as a function of x for a bimaterial with $\beta_2 = 3\beta_1$ and $\beta_1 = 10^{-2}$.

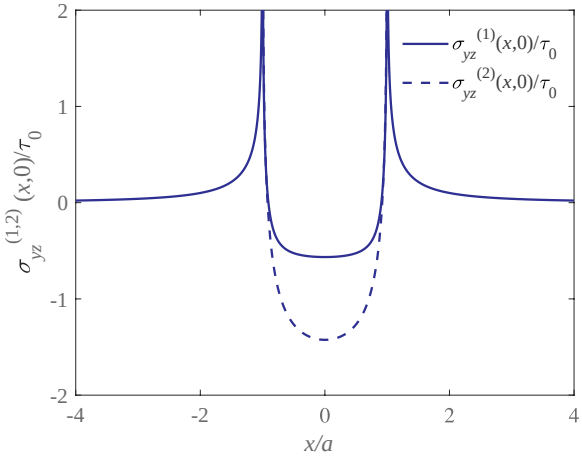

Fig. 7. Variation of the bulk stresses at the crack line as a function of x for a bimaterial with $\beta_2 = 3\beta_1$ and $\beta_1 = 10^{-1}$.

$\mu_1^s/\mu_1 = 10^{-10}m$, when the crack half-length is lower than $10\mu m$, the surface effect comes into play and rapidly decreases the stress intensity factors. In other words, the load-carrying capacity is effectively enhanced with consideration of surface effect (Zhang et al., 2014). In particular, if neglecting the surface elasticity, we find that the normalized stress intensity factors are equal to unity. That is, when the crack half-length increases to the millimeter-order length or more, the surface effect is nearly invisible and the classical stress intensity factor is recovered. When the crack length decreases to the micrometer-order

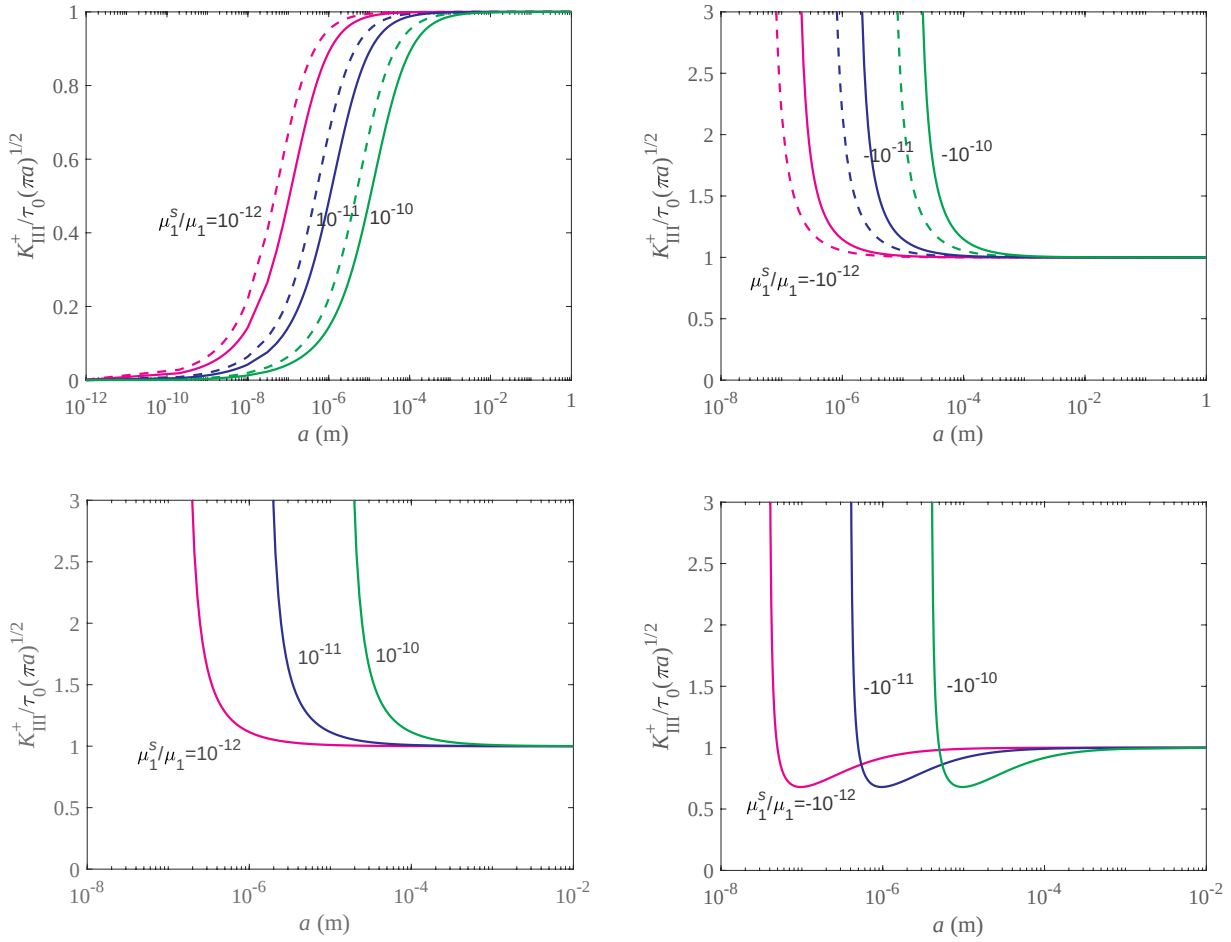

Fig. 8. Dimensionless stress intensity factor $K^{\pm}_{III}/\tau_0\sqrt{\pi a}$ against the crack half-length a with $|\beta_2| = 3|\beta_1|$, a) positive μ_1^s/μ_1 and μ_2^s/μ_2, b) negative μ_1^s/μ_1 and μ_2^s/μ_2, c) $\mu_1^s/\mu_1 > 0$ and $\mu_2^s/\mu_2 < 0$, d) $\mu_1^s/\mu_1 < 0$ and $\mu_2^s/\mu_2 > 0$ where the dashed lines and the solid lines correspond to an identical material and a bimaterial, respectively.

length or less, the influence of surface elasticity on the classical stress intensity factor is pronounced and cannot be neglected. It also shows that positive surface shear moduli decrease the stress intensity factors, and then impedes crack advance. This conclusion agrees well with most experimental observation (Cohen-Tanugi and Grossman, 2014; Yang et al., 2010). Although the values of μ_1^s and μ_2^s are positive for most materials, it is worth noting that negative μ_1^s and μ_2^s values are still possible for some special crystalline directions. Fig. 8b gives the variation of stress intensity factors with $\mu_1^s, \mu_2^s < 0$. From Fig. 8b, negative surface material parameters may increase the stress intensity factors and then speed the crack advance, which is opposite to the trend for positive surface material parameters. Some more complex behaviors can be observed in Fig. 8(c,d), which illustrates the variation of the normalized stress intensity factors for other combined cases of a positive and a negative surface modulus. Through the above analysis, both the surface parameters μ_1^s and μ_2^s strongly influence the behavior of stress intensity factors and then affect the effective interface fracture toughness of a bimaterial.

Fig. 9 shows the variation of the dimensionless stress intensity factors against the dimensionless surface parameter β_1 for different β_2 values. From Fig. 9a, it is viewed that when the surface parameters β_1 and β_2 increase, the stress intensity factors decrease. It also implies a higher load-carrying capacity when considering surface effects. For other combined cases of β_1 and β_2, stress intensity factors as a function of β_1 are displayed in Figs. 9b-d for various values of β_2. Their variations are similar to those in Fig. 8.

6. Conclusions

In this paper, we analyzed a nanoscale mode-III interface crack of two bonded dissimilar isotropic homogeneous media. The influences of surface elasticity on the crack-tip field were examined. With the aid of the Fourier transform, we derived a hypersingular integro-differential equation for the out-of-plane displacement jump and bulk stress jump across the crack faces. To employ the Galerkin method to solve the resulting equation, we used the Chebyshev polynomials to expand the displacement and stress jumps. The set of resulting hypersingular integro-differential equations was converted to a set of algebraic equations with unknown coefficients. The stress intensity factors were computed and presented for different surface properties. The obtained results show that for most materials with positive β_1 and β_2 parameters, consideration of surface elasticity decreases the stress intensity factor or the effective fracture toughness is enhanced for materials with nano/microscale crack. Conversely, negative β_1 and β_2 values increase the stress intensity factors or reduce the effective fracture toughness. A combined case of β_1 and β_2 causes the stress intensity factors to exhibit more complex variation.

Declaration of Competing Interest

The authors declare that they have no conflict of interest.

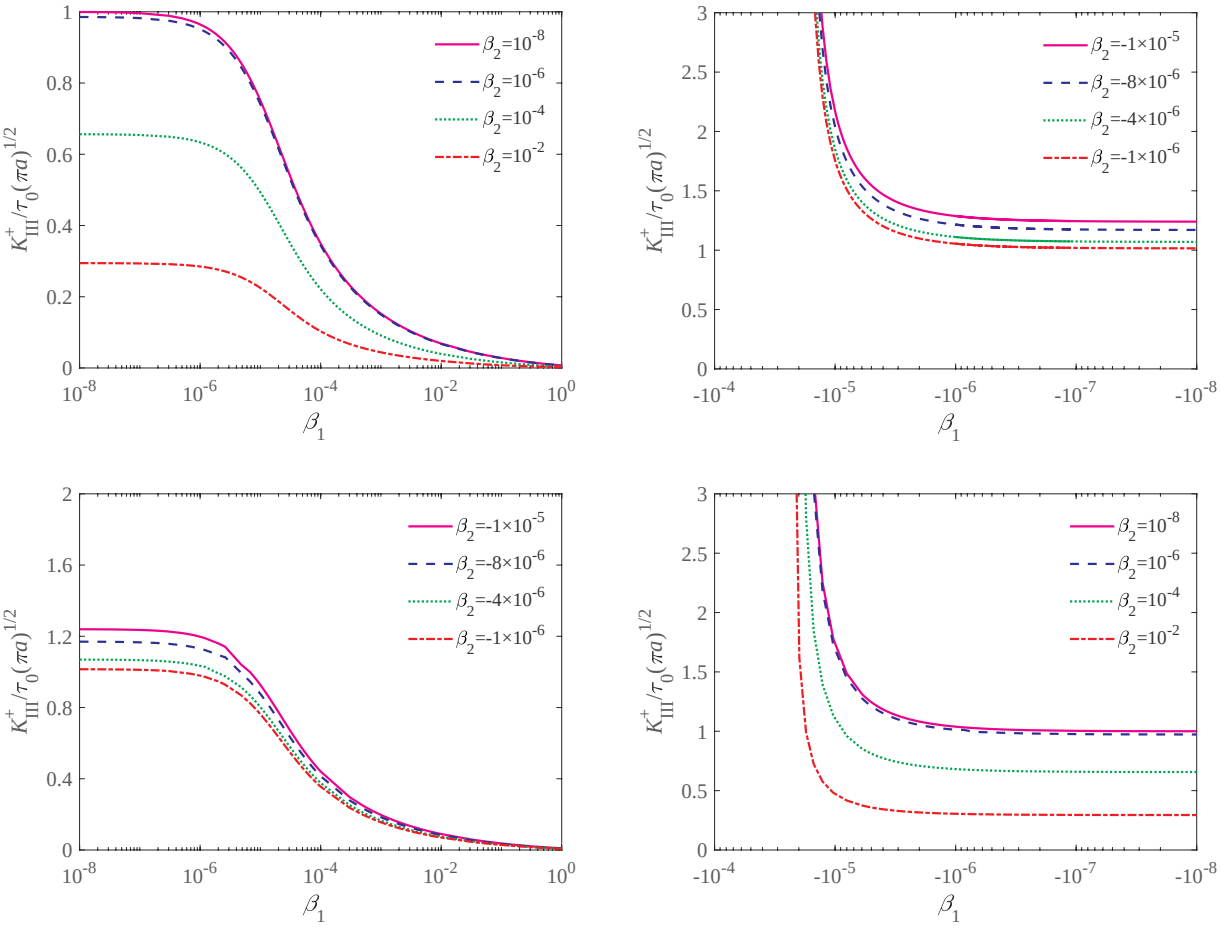

Fig. 9. Dimensionless stress intensity factor $K_{III}^{\pm}/\tau_0\sqrt{\pi a}$ against the surface parameters β_1, a) $\mu_1^s/\mu_1 > 0$ and $\mu_2^s/\mu_2 > 0$, b) $\mu_1^s/\mu_1 < 0$ and $\mu_2^s/\mu_2 < 0$, c) $\mu_1^s/\mu_1 > 0$ and $\mu_2^s/\mu_2 < 0$, d) $\mu_1^s/\mu_1 < 0$ and $\mu_2^s/\mu_2 > 0$.

Acknowledgments

The authors would be grateful to the Editor-in-Chief, Professor Benjamin Loret, and three anonymous reviewers for their helpful suggestions in improving the original manuscript. This work was supported by the National Natural Science Foundation of China (Grant No. 11672336) and the Fundamental Research Funds for the Central Universities of Central South University (No. 2019zzts872).

Appendix A

A further simplification is achieved by multiplying (46) by μ_2 and multiplying (47) by μ_1. Then adding them results in

$$\frac{\beta_2-\beta_1}{\pi}\int_{-1}^{1}\frac{\bar{h}(\bar{s})}{(\bar{s}-\bar{x})^2}d\bar{s}+(\mu_1\beta_2+\mu_2\beta_1)\bar{g}''(\bar{x})+\frac{\mu_1+\mu_2}{\pi}\int_{-1}^{1}\frac{\bar{g}(\bar{s})}{(\bar{s}-\bar{x})^2}d\bar{s}=\frac{1}{2}\left(2+\frac{\mu_1}{\mu_2}+\frac{\mu_2}{\mu_1}\right)\tau_0\zeta(\bar{x}). \tag{A.1}$$

To eliminate hypersingular kernels in the above equation, integrating both sides of the above hypersingular integro-differential equation leads to a singular integro-differential equation with the Cauchy kernel, namely

$$\frac{1}{\pi}\int_{-1}^{1}\frac{\bar{g}(\bar{s})}{\bar{s}-\bar{x}}d\bar{s}+\frac{\mu_1\beta_2+\mu_2\beta_1}{\mu_1+\mu_2}\bar{g}'(\bar{x})+\frac{\beta_2-\beta_1}{\pi(\mu_1+\mu_2)}\int_{-1}^{1}\frac{\bar{h}(\bar{s})}{\bar{s}-\bar{x}}d\bar{s}=\frac{1}{2}\tau_0\left(\frac{1}{\mu_1}+\frac{1}{\mu_2}\right)\zeta^*(\bar{x}),\quad |\bar{x}|<1, \tag{A.2}$$

where

$$\zeta^*(\bar{x})=\int_0^{\bar{x}}\zeta(\bar{s})d\bar{s}. \tag{A.3}$$

In the above derivation, we have used the condition that an integration constant is taken as zero since $\bar{g}(\bar{x})$ and $\bar{h}(\bar{x})$ are even functions, $\bar{g}'(\bar{x})$ is an odd function. In addition, the singular integral operator $\int_{-1}^{1}\bar{h}(\bar{s})/(\bar{s}-\bar{x})d\bar{s}$ transforms an even function to an odd function.

On the other hand, from Eqs. (46) and (47) we eliminate $\bar{g}''(\bar{x})$ and, after some manipulations, obtain

$$\frac{\mu_1\beta_2+\mu_2\beta_1}{\mu_1+\mu_2}\bar{h}(\bar{x})-\frac{\beta_1\beta_2}{\pi}\int_{-1}^{1}\frac{\bar{h}(\bar{s})}{(\bar{s}-\bar{x})^2}d\bar{s}+\frac{\beta_2-\beta_1}{\pi(\mu_1^{-1}+\mu_2^{-1})}\int_{-1}^{1}\frac{\bar{g}(\bar{s})}{(\bar{s}-\bar{x})^2}d\bar{s}=\frac{1}{2}(\beta_2-\beta_1)\tau_0\zeta(\bar{x}). \tag{A.4}$$

Appendix B

We rewrite Eq. (A.2) as

$$\frac{1}{\pi}\int_{-1}^{1}\frac{1}{\bar{s}-\bar{x}}\left[\bar{g}(\bar{s})+\frac{\beta_2-\beta_1}{\pi(\mu_1+\mu_2)}\bar{h}(\bar{s})\right]d\bar{s}=\frac{\tau_0}{2}\left(\frac{1}{\mu_1}+\frac{1}{\mu_2}\right)\zeta^*(\bar{x})-\frac{\mu_1\beta_2+\mu_2\beta_1}{\mu_1+\mu_2}\bar{g}'(\bar{x}). \tag{B1}$$

It can be understood as a singular integral equation with the Cauchy kernel of the first kind (Muskhelishvili, 1977). Under the conditions (45) and with the aid of the well-known solution of singular integral equations with the Cauchy kernel of the first kind, we arrive at the following result

$$\bar{g}(\bar{x})+\frac{\beta_2-\beta_1}{\pi(\mu_1+\mu_2)}\bar{h}(\bar{x})=-\frac{\sqrt{1-\bar{x}^2}}{\pi}\int_{-1}^{1}\frac{\frac{\tau_0}{2}\left(\frac{1}{\mu_1}+\frac{1}{\mu_2}\right)\zeta^*(\bar{s})-\frac{\mu_1\beta_2+\mu_2\beta_1}{\mu_1+\mu_2}\bar{g}'(\bar{s})}{(\bar{s}-\bar{x})\sqrt{1-\bar{s}^2}}d\bar{s}, \tag{B2}$$

and

$$\int_{-1}^{1}\frac{\frac{\tau_0}{2}\left(\frac{1}{\mu_1}+\frac{1}{\mu_2}\right)\zeta^*(\bar{s})-\frac{\mu_1\beta_2+\mu_2\beta_1}{\mu_1+\mu_2}\bar{g}'(\bar{s})}{\sqrt{1-\bar{s}^2}}d\bar{s}=0. \tag{B3}$$

Similar to the above treatment we also integrate both sides of Eq. (A.4)to obtain

$$\frac{\beta_2-\beta_1}{\pi(\mu_1^{-1}+\mu_2^{-1})}\int_{-1}^{1}\frac{\bar{g}(\bar{s})}{\bar{s}-\bar{x}}d\bar{s}-\frac{\beta_1\beta_2}{\pi}\int_{-1}^{1}\frac{\bar{h}(\bar{s})}{\bar{s}-\bar{x}}d\bar{s}=\frac{1}{2}(\beta_2-\beta_1)\tau_0\zeta^*(\bar{x})-\frac{\mu_1\beta_2+\mu_2\beta_1}{\mu_1+\mu_2}\int_0^{\bar{x}}\bar{h}(\bar{s})d\bar{s}. \tag{B4}$$

Likely, we have

$$\frac{\beta_2-\beta_1}{(\mu_1^{-1}+\mu_2^{-1})}\bar{g}(\bar{x})-\beta_1\beta_2\bar{h}(\bar{x})=-\frac{\sqrt{1-\bar{x}^2}}{\pi(\mu_1+\mu_2)}\int_{-1}^{1}\frac{\frac{1}{2}(\mu_1+\mu_2)(\beta_2-\beta_1)\tau_0\zeta^*(\bar{s})-(\mu_1\beta_2+\mu_2\beta_1)\int_0^{\bar{s}}\bar{h}(t)dt}{(\bar{s}-\bar{x})\sqrt{1-\bar{s}^2}}d\bar{s}, \tag{B5}$$

and

$$\int_{-1}^{1}\frac{\frac{1}{2}(\mu_1+\mu_2)(\beta_2-\beta_1)\tau_0\zeta^*(\bar{s})-(\mu_1\beta_2+\mu_2\beta_1)\int_0^{\bar{s}}\bar{h}(t)dt}{\sqrt{1-\bar{s}^2}}d\bar{s}=0. \tag{B6}$$

Appendix C

Recalling the closed-form integral formula

$$\frac{1}{\pi}\int_{-1}^{1}\frac{U_n(\bar{s})\sqrt{1-\bar{s}^2}}{\bar{s}-\bar{x}}d\bar{s}=-T_{n+1}(\bar{x}),\quad |\bar{x}|<1, \tag{B1}$$

and derivative formula

$$\frac{dU_n(\bar{x})}{d\bar{x}}=\frac{(n+2)U_{n-1}(\bar{x})-nU_{n+1}(\bar{x})}{2(1-\bar{x}^2)} \tag{B2}$$

we obtain

$$\frac{d}{d\bar{x}}[U_n(\bar{x})\sqrt{1-\bar{x}^2}]=(n+1)\frac{U_{n-1}(\bar{x})-U_{n+1}(\bar{x})}{2\sqrt{1-\bar{x}^2}}=-\frac{(n+1)T_{n+1}(\bar{x})}{\sqrt{1-\bar{x}^2}}. \tag{B3}$$

Bearing this result in mind, one inserts (50) and (51) into Eq. (A.2), leading to

$$\sum_{n=0}^{N}b_n\left(\frac{\mu_1\beta_2+\mu_2\beta_1}{\mu_1+\mu_2}\frac{n+1}{\sqrt{1-\bar{x}^2}}+1\right)T_{n+1}(\bar{x})+\frac{\mu_1\mu_2(\beta_2-\beta_1)}{(\mu_1+\mu_2)^2}\sum_{n=0}^{N}c_nT_{n+1}(\bar{x})=-\zeta^*(\bar{x}). \tag{B4}$$

We multiply both sides of Eq. (C.4) by $T_{m+1}(x)$, and then integrate both sides with respect to x from -1 to 1. Applying the orthogonality of the Chebyshev polynomials

$$\int_{-1}^{1}\frac{T_m(\bar{x})T_n(\bar{x})}{\sqrt{1-\bar{x}^2}}d\bar{x}=\begin{cases}0, & m\neq n,\\ \pi, & m=n=0,\\ \frac{\pi}{2}, & m=n,\ m\neq 0,\end{cases} \tag{B5}$$

and the closed-form integral formula

$$\int_{-1}^{1}T_m(\bar{x})T_n(\bar{x})d\bar{x}=\frac{1+(-1)^{m-n}}{2}\left[\frac{1}{1-(m-n)^2}+\frac{1}{1-(m+n)^2}\right], \tag{B6}$$

from (C.4) we obtain linear algebraic equations for the unknown constants b_n and c_n $(n=0,\ 1,\ ...,N)$

$$\sum_{n=0}^{N}\left[\frac{\mu_1\beta_2+\mu_2\beta_1}{\mu_1+\mu_2}\frac{(n+1)\pi}{2}\delta_{mn}+a_{mn}^{+}\right]b_n+\frac{\mu_1\mu_2(\beta_2-\beta_1)}{(\mu_1+\mu_2)^2}\sum_{n=0}^{N}a_{mn}^{+}c_n=-f_{1m},\quad m=0,\ 1,\ ...N. \tag{B7}$$

Next, we substitute the expansions (50) and (51) into equation (A.4). Recalling the closed-form hypersingular integral formula (63) we obtain

$$\sum_{n=0}^{N} c_n \left[\frac{\mu_1\beta_2 + \mu_2\beta_1}{\mu_1 + \mu_2}\sqrt{1-\bar{x}^2} + (n+1)\beta_1\beta_2 \right] U_n(\bar{x}) - (\beta_2 - \beta_1) \sum_{n=0}^{N} b_n(n+1)U_n(\bar{x}) = (\beta_2 - \beta_1)\zeta(\bar{x}). \tag{C.8}$$

After multiplying both sides of Eq. (C.8) by $U_m(\bar{x})\sqrt{1-\bar{x}^2}$ $(m \geq 0)$ and then integrating both sides with respect to $\bar{x}$ from -1 to 1, with the aid of the orthogonality of Chebyshev polynomials of the second kind and closed-form integral result

$$\int_{-1}^{1} \sqrt{1-\bar{x}^2}\, U_m(\bar{x})U_n(\bar{x})d\bar{x} = \frac{\pi}{2}\delta_{mn}, \tag{C.9}$$

$$\int_{-1}^{1} (1-\bar{x}^2)U_m(\bar{x})U_n(\bar{x})d\bar{x} = \frac{1+(-1)^{m-n}}{2}\left[\frac{1}{1-(m-n)^2} - \frac{1}{1-(m+n+2)^2} \right]. \tag{C.10}$$

we obtain linear algebraic equations for the unknown constants b_n and c_n $(n = 0, 1, ...,N)$

$$-\sum_{n=0}^{N} \frac{(n+1)\pi}{2}(\beta_2 - \beta_1)\delta_{mn}b_n + \sum_{n=0}^{N} \left[\frac{\mu_1\beta_2 + \mu_2\beta_1}{\mu_1 + \mu_2}\bar{a_{mn}} + \frac{(n+1)\pi}{2}\beta_1\beta_2\delta_{mn} \right] c_n = (\beta_2 - \beta_1)f_{2m}, \quad m = 0, 1, ...N. \tag{C.11}$$

Supplementary material

Supplementary material associated with this article can be found, in the online version, at 10.1016/j.mechmat.2019.103246.

References

Chan, Y.S., Fannjiang, A.C., Paulino, G.H., 2003. Integral equations with hypersingular kernels–theory and applications to fracture mechanics. Int. J. Eng. Sci. 41 (7), 683–720.

Chen, T., Chiu, M.-S., Weng, C.N., 2006. Derivation of the generalized Young-Laplace equation of curved interfaces in nanoscaled solids. J. Appl. Phys. 100 (7), 074308.

Cohen-Tanugi, D., Grossman, J.C., 2014. Mechanical strength of nanoporous graphene as a desalination membrane. Nano Lett. 14 (11), 6171.

Del Rio, F.W., Cook, R.F., Boyce, B.L., 2015. Fracture strength of micro- and nano-scale silicon components. Appl. Phys. Rev. 2 (2), 021303.

Dingreville, R., Qu, J., Cherkaoui, M., 2005. Surface free energy and its effect on the elastic behavior of nano-sized particles, wires and films. J. Mech. Phys. Solids 53 (8), 1827–1854.

Duan, H.L., Wang, J., Karihaloo, B.L., 2009. Theory of elasticity at the nanoscale. Adv. Appl. Mech. 1–68.

England, A.H., 1965. A crack between dissimilar media. J. Appl. Mech. 32, 400–402.

Fu, X.L., Wang, G.F., Feng, X.Q., 2008. Surface effects on the near-tip stress fields of a mode-II crack. Int. J. Fract. 151 (2), 95–106.

Gao, X., Hao, F., Fang, D., Huang, Z., 2013. Boussinesq problem with the surface effect and its application to contact mechanics at the nanoscale. Int. J. Solids Struct. 50 (16–17), 2620–2630.

Gao, X., Hao, F., Huang, Z., Fang, D., 2014. Mechanics of adhesive contact at the nanoscale: the effect of surface stress. Int. J. Solids Struct. 51 (3–4), 566–574.

Gurtin, M.E., Murdoch, A.I., 1975. A continuum theory of elastic material surfaces. Arch. Ration. Mech. Anal. 57 (4), 291–323. 59: 389–390

Gurtin, M.E., Weissmüller, J., Larché, F., 1998. A general theory of curved deformable interfaces in solids at equilibrium. Philos. Mag. A 78 (5), 1093–1109.

Hori, M., Nemat-Nasser, S., 1990. Asymptotic solution of a class of strongly singular integral equations. SIAM J. Appl. Math. 50 (3), 716–725.

Hu, K.-M., Zhang, W.-M., Peng, Z.-K., Meng, G., 2015. Transverse vibrations of mixed-mode cracked nanobeams with surface effect. J. Vib. Acoust. 138 (1), 011020.

Hu, K.-M., Zhang, W.-M., Zhong, Z.-Y., Peng, Z.-K., Meng, G., 2014. Effect of surface layer thickness on buckling and vibration of nonlocal nanowires. Phys. Lett. A 378 (7), 650–654.

Hu, Z.-L., Lee, K.Y., Li, X.F., 2018. Crack in an elastic thin-film with surface effect. Int. J. Eng. Sci. 123, 158–173.

Hu, Z.-L., Li, X.F., 2018. A rigid line inclusion in an elastic film with surface elasticity. Z. Angew. Math. Phys. 69, 92.

Kaya, A.C., Erdogan, F., 1987. On the solution of integral equations with strongly singular kernels. Q. Appl. Math. 45 (1), 105–122.

Kim, C., Ru, C.-Q., Schiavone, P., 2013. A clarification of the role of crack-tip conditions in linear elasticity with surface effects. Math. Mech. Solids 18 (1), 59–66.

Kim, C.I., Schiavone, P., Ru, C.Q., 2010. The effects of surface elasticity on an elastic solid with mode-III crack: Complete solution. J. Appl. Mech. 77 (2), 021011.

Kim, C.I., Schiavone, P., Ru, C.Q., 2011. Analysis of plane-strain crack problems mode-I and mode-II in the presence of surface elasticity. J. Elast. 104 (1–2), 397–420.

Kim, C.I., Schiavone, P., Ru, C.Q., 2011. The effect of surface elasticity on a mode-III interface crack. Arch. Mech. 63 (3), 267–286.

Kim, C.I., Schiavone, P., Ru, C.Q., 2011. Effect of surface elasticity on an interface crack in plane deformations. Proc. R. Soc. A 467 (2136), 3530–3549.

Li, X.F., 2019. Effect of surface elasticity on stress intensity factors near the mode-III crack tips. J. Mech. Mater. Struct. 14 (1), 43–60.

Li, X.-F., Tang, G.-J., Shen, Z.-B., Lee, K.Y., 2015. Axisymmetric problems of a penny-shaped crack at the interface of a bi-material under shear and compression. Int. J. Solids Struct. 69–70, 403–414.

Li, X.F., Tang, G.J., Shen, Z.B., Lee, K.Y., 2015. Interface crack embedded in a bi-material plane under shear and compression. Mech. Mater. 85, 80–93.

Li, X.F., Tang, G.J., Tang, B.Q., 2013. Stress field around a strike-slip fault in orthotropic elastic layers via a hypersingular integral equation. Comput. Math. Appl. 66 (11), 2317–2326.

Martin, P.A., 1992. Exact solution of a simple hypersingular integral equation. J. Integral Eq. 4, 197–204.

Mogilevskaya, S.G., Crouch, S.L., Stolarski, H.K., 2008. Multiple interacting circular nano-inhomogeneities with surface/interface effects. J. Mech. Phys. Solids 56 (6), 2298–2327.

Murdoch, A.I., 1976. The propagation of surface waves in bodies with material boundaries. J. Mech. Phys. Solids 24, 137–146.

Muskhelishvili, N.I., 1977. Some Basic Problems of the Mathematical Theory of Elasticity: Fundamental Equations Plane Theory of Elasticity Torsion and Bending. Springer, Netherlands.

Nan, H., Wang, B., 2012. Effect of residual surface stress on the fracture of nanoscale materials. Mech. Res. Commun. 44, 30–34.

Ru, C.Q., 2010. Simple geometrical explanation of Gurtin-Murdoch model of surface elasticity with clarification of its related versions. Sci. China A 53 (3), 536–544.

Sharma, P., Ganti, S., 2004. Size-dependent Eshelby's tensor for embedded nano-inclusions incorporating surface/interface energies. J. Appl. Mech. 71 (4), 663–671.

Shenoy, V.B., 2005. Atomistic calculations of elastic properties of metallic FCC crystal surfaces. Phys. Rev. B 71 (9), 094104.

Walton, J.R., 2012. A note on fracture models incorporating surface elasticity. J. Elast. 109 (1), 95–102.

Wang, B.L., Wang, K.F., 2013. Effect of surface residual stress on the fracture of double cantilever beam fracture toughness specimen. J. Appl. Phys. 113 (15), 153502.

Wang, G.F., Feng, X.Q., 2007. Effects of surface stresses on contact problems at nanoscale. J. Appl. Phys. 101 (1), 013510.

Wang, G.F., Feng, X.Q., Wang, T.J., Gao, W., 2008. Surface effects on the near-tip stresses for mode-I and mode-III cracks. J. Appl. Mech. 75 (1), 011001.

Wang, H., Li, X., Tang, G., Shen, Z., 2013. Effect of surface stress on stress intensity factors of a nanoscale crack via double cantilever beam model. J. Nanosci. Nanotechnol. 13 (1), 477–482.

Wu, C.H., 1999. The effect of surface stress on the configurational equilibrium of voids and cracks. J. Mech. Phys. Solids 47 (12), 2469–2492.

Xiao, Q.-X., Li, X.-F., 2018. Flutter and divergence instability of rectangular plates under nonconservative forces considering surface elasticity. Int. J. Mech. Sci. 149, 254–261.

Yang, P., Li, C., Shang, S., Zhang, L., 2010. Nano-indentation test and numerical evaluation of Cu-Cr interface structure in micro/nano manufacturing. Compos. Interfaces 17 (8), 789–801.

Yang, Y., Li, X.F., 2019. Bending and free vibration of a circular magnetoelectroelastic plate with surface effects. Int. J. Mech. Sci. 157–158, 858–871.

Yao, H., Yun, G., 2012. The effect of nonuniform surface elasticity on buckling of ZnO nanowires. Physica E 44 (9), 1916–1919.

Zhang, P., Ma, L., Fan, F., Zeng, Z., Cheng, P., Loya, P.E., Liu, Z., Gong, Y., Zhang, J., Zhang, X., 2014. Fracture toughness of graphene. Nat. Commun. 5 (4), 3782.

Zhang, W.-M., Hu, K.-M., Yang, B., Peng, Z.-K., Meng, G., 2016. Effects of surface relaxation and reconstruction on the vibration characteristics of nanobeams. J. Phys. D 49 (16), 165304.